

MoEDAL MAPP detector for detection of physics beyond the Standard Model at the LHC - progress report

Alejandro Salazar Lobos, ID: 1517982^{1,*}

¹*Department of Physics, University of Alberta, Edmonton, AB, Canada T6G 2G7*

Abstract

One of the methods for detecting particles at the MAPP detector of the MoEDAL experiment at the LHC is via the reconstruction of decay vertices from incoming particles. The preliminary study offered in this report found that, for neutral particles, decay vertices could be reconstructed to a resolution of 0.069 ± 0.005 m. In addition, a progress report is given on the testing of the performance of the equipment.

*Electronic address: aasalaza@ualberta.ca

I. INTRODUCTION

The Standard Model of particle physics has kept its ground since 1978. The current picture is that all matter is made of three kinds of elementary particles: leptons (three generations: electron, muon, and tauon), quarks (six flavours: u, c, t, and d, s, b), and mediators (the photon for the electromagnetic interaction, the W's and Z for the weak interaction, the gluon for the strong interaction, and the [hypothetical] graviton for the gravitational interactions). [8] Over the past 42 years, the Standard Model has been tested rigorously. It has had its triumphs with certain discoveries, for example, among the most remarkable, the discovery of the neutral current interactions in 1973 [9, 10] and the discovery of the Higgs boson (necessary for the masses of the W's and Z) in 2012 [1, 4], both predicted by the Glashow-Weinberg-Salam electroweak theory. But there are many issues for which the Standard Model does not provide an answer. For example, it does not tell us how to calculate the masses of the quarks and leptons [8]; it also predicts massless neutrinos, which was proven wrong with the discovery of neutrino oscillations in 2005 [12]. There are too many free parameters in the standard model, and a lot of quantities must be introduced by hand. The Standard Model is far from being complete as an explanation of the elementary constituents of matter. The discovery of neutrino oscillations, for example, is a clear evidence that there could be more physics beyond the Standard Model.

The Monopole & Exotics Detector at the Large Hadron Collider (MoEDAL) is an experiment that looks for physics beyond the standard model. The MoEDAL main detector is designed primarily for the search of magnetic monopoles and other highly ionizing particles produced from high-energy collisions at the LHC. [2] The MoEDAL Apparatus for Penetrating Particles (MAPP) is a subdetector of the MoEDAL experiment. MAPP is designed to detect fractionally-charged particles and long-lived neutral particles. [14] In particular, MAPP could possibly detect heavy neutrinos (see Section II). Part of the identification of particles at MAPP is done via the reconstruction of decay vertices. This report provides preliminary results of the simulation of the decay of particles to be detected at MAPP, and determines a resolution for the reconstruction of their decay vertices; it also gives preliminary results on the testing of the equipment and the setup that could be used.

II. THEORY

The MoEDAL experiment considers the possibility of the existence of heavy neutrinos, which detection at the LHC would occur by ionization processes caused by a large electric dipole moment (EDM) of the neutrino. [6] Currently, the bounds for heavy neutral leptons require a mass larger than 45 GeV for the heavy neutrino; [6, 16] it is known, however, that the mass of the tau neutrino, the heaviest of the three known lepton generations, is less than 18 MeV [8], and that the number of light neutrinos is 2.9841 ± 0.0083 [3]; in addition, the experiments so far show that the lifetime of the Z^0 is consistent with three generations of light neutrinos [8]. The existence of a neutrino with a mass larger than 45 GeV would therefore require a new lepton generation(s). In fact, the existence of a fourth lepton generation, with a neutrino of mass larger than 45 GeV, would require masses that might be too heavy to affect the lifetime of the Z^0 [8], which further supports the possible existence of this fourth generation.

The addition of a fourth lepton generation to the Standard Model would not be trivial, and it is ruled out by the Higgs data. [6, 7] A model (Ishiwata and Wise) suggests that a fourth generation of leptons would leave the decay modes of the Higgs untouched, except for the modes $H \rightarrow \gamma\gamma$, γZ , and gg . [6, 11] These altered modes could be induced by gauge boson and heavy-fermion loops, and if the heavy neutrinos are light enough, then the Higgs boson would be allowed to decay to particles not predicted by the Standard Model. [6, 11] So the discovery of heavy neutrinos would open the doors to the possibility of the existence of more beyond the Standard Model particles. Based on this information, the MoEDAL experiment considers the existence of a fourth generation of leptons, which gives a heavy neutrino belonging to a fourth leptonic SU(2) isodoublet [6], giving its charged partner a mass greater than 100.8 GeV [6, 16].

A parallel can be built between the magnetic dipole moment, generated from an infinitesimally small loop of electric charge, and an EDM arising from an infinitesimally small loop of magnetic charge (this further supports the possible existence of magnetic monopoles). The Hamiltonian arising from the interaction of electric and magnetic dipole moments, d and μ , of a moving particle, with external fields is given by the Hamiltonian: [15]

$$H = \frac{-d\mathbf{E}^0 \cdot \mathbf{S} - \mu\mathbf{B}^0 \cdot \mathbf{S}}{\gamma}, \quad (1)$$

where \mathbf{E}^0 and \mathbf{B}^0 are the fields in the instantaneously accompanying frame of the moving particle, γ is the usual relativistic factor, and \mathbf{S} is a dimensionless factor arising from angular momentum. In the rest frame of the particle, $d \neq 0$ only when CP invariance is violated. [15] Thus the prediction: the existence of an EDM requires CP violation (or T violation by the TCP theorem [8]), which can give rise to distinct possible Feynman diagrams for its generation.

For a neutral particle with an EDM, the energy loss from (in our case weak and electromagnetic) interactions is given by: [6]

$$\frac{dE}{dx} = \pi N Z \frac{e^2}{4\pi\epsilon_0} D\gamma, \quad (2)$$

where Z is the nuclear charge, N is the neutron number, γ is the relativistic factor, e is the charge of the electron, and ϵ_0 is the vacuum permittivity. MoEDAL has determined that the heavy neutrino would be detected due to its EDM if it gives rise to the production of 100 photons via ionization process in the scintillator material in each section of the MAPP detector. [6] It is assumed that 10^4 photons are produced per MeV energy deposited in the scintillator; for comparison with other MoEDAL detectors, it is assumed that the MAPP detector is 100% efficient. [6] This project explores the possibility of the detection of particles at MAPP via the reconstruction of their decay vertices, which will be added to the detection process explained above for the overall MAPP project. It also gives a progress report on the determination of the efficiency of the scintillator material to be used at MAPP.

Scintillator plastics are made of an aromatic plastic or a compound of non-aromatic plastic with an aromatic co-solvent (common materials are polystyrene [PS] and polyvhtyltoluene [PVT]). [5, 13] The plastic itself has an emission spectrum of 300-350 nm, which is too short for commonly used photodetectors; this is fixed by adding 1% weight of primary fluor and an additional 0.01% weight of a spectrum shifter (an additional fluorescent compound), which generate a blue to blue-green (400-500 nm) emission spectrum. [13] ‘sp²’ hybridization in the plastic occurs from carbon bonding; in this electronic configuration one of the four valence electrons (called ‘π electrons’) becomes delocalized from the molecule; this phenomenon leads to fluorescence, which occurs from a transition from spin singlet excited states to singlet ground states of the ‘π-electron’ system. [5] All this process can be triggered from the interaction of the molecules with a charged particle. [5] Highly ionizing particles are expected to have the same effect, and specially, EDM particles are expected to interact by

ionization with the scintillator plastic via electric interactions.

III. EXPERIMENTAL DETAILS

A. Exploration of the resolution in the reconstruction of decay vertices at the LHC

1. *The MAPP detector*

This project is part of the experiment to be conducted using the MAPP subdetector of the bigger MoEDAL detector at the LHC. Part of the detection of particles would be made through the reconstruction of decay vertices. The basic setup of the MAPP detector will be three boxes of different size made of scintillating material (acrylic plastic) (for an explanation of the workings of the scintillator, look at Section II). The largest box will enclose the medium-size box, and this one will enclose the smallest one. The boxes will be missing a face, allowing the decay products to enter the ‘detection zone’ (i.e. the area inside the boxes). Before this, the decaying particle must cross a veto. The veto is a wall of scintillating acrylic plastic that will tell whether the decay vertex occurred inside the ‘decay zone’ (i.e. the area between the veto wall and the boxes). In addition to this, MAPP assures that only long-lived neutral particles, and fractionally-charged particles make it passed the veto zone; this is achieved by having MAPP protected from Standard Model particles by about 30 to 55 meters of rock, and from cosmic rays by being underneath roughly 100 meters of limestone. [14] See Figure 1 for a diagram of the location of the MAPP detector at the LHC. For this paper, walls instead of boxes were used as a preliminary study for the reconstruction of decay vertices and the resolution one can achieve for such reconstructions. Figure 2 shows the setup of the MAPP detector for three detection planes.

2. *The detection planes*

For the following description, please refer to Figure 2. This is a preliminary study, and the dimensions can be subjected to change. The detection planes are made of an array of 3 m long and 3 cm wide scintillator planks. In order to make a detection wall, a set of these planks is placed vertically, with the planks overlapped by 1 cm along the x axis; the

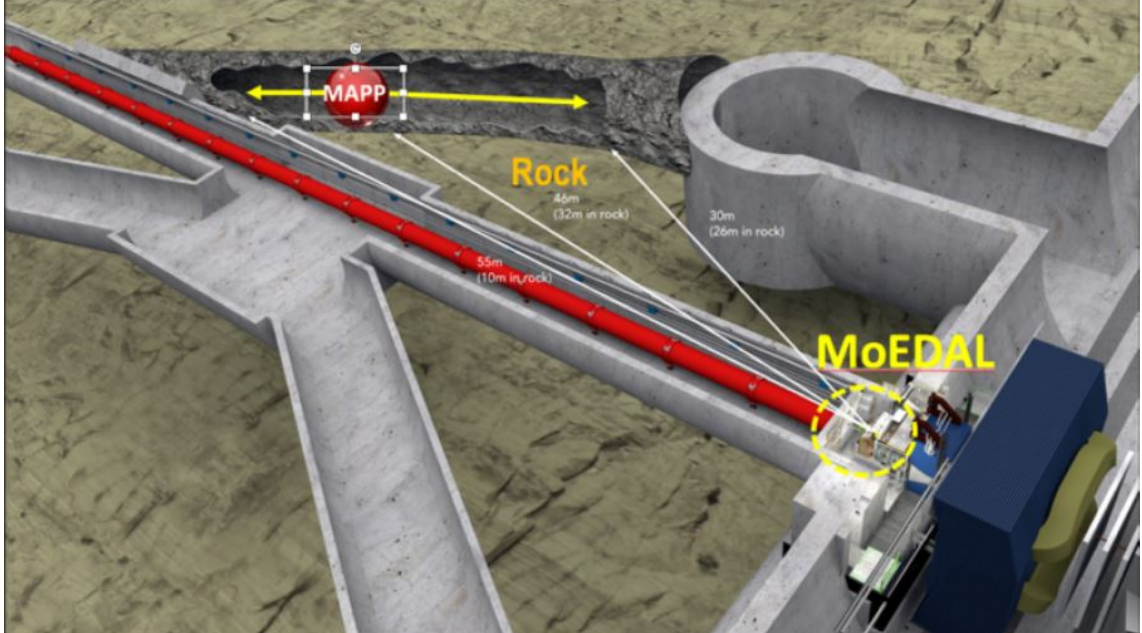


FIG. 1: Impression of the deployment of the MAPP detector in the UGC8 gallery adjacent to the main MoEDAL detector at the LHC. Taken from [14].

other set is placed horizontally and overlapped by 1cm along the y axis. Figure 3 shows a diagram of how the overlapping of the planks looks as seen from one end. In this way, each detection wall becomes, effectively, $3 \text{ m} \times 3 \text{ m}$ grid made up of $1 \text{ cm} \times 1 \text{ cm}$ detection squares (see Figure 4). The overlapping of the scintillator strips allows the experimentalists to know through which detection square the particle passed. For example, if only the scintillator on the far left of Figure 3 is triggered, then we know that the particle passed through only that strip; if the far-left strip and the strip in the middle are triggered, then we know that the particle passed through the two of them. Doing this for both axes, x and y in Figure 2, and for an array of overlapped scintillator strips making up a wall of $3 \times 3 \text{ m}^2$, we can tell which detection square in Figure 4 the particle crossed.

The simulation for the reconstruction of vertices was done as follows, and it is summarized in Figure 5: a decay vertex (which I call the ‘reference vertex’) was created half-way through the ‘decay zone’ (in Figure 2, $x = 1.50 \text{ [m]}$, $y = 1.5 \text{ [m]}$, $z = -2.50 \text{ [m]}$; see Figure 5a). It was assumed that the decaying particle moves parallel to the negative z axis, and that two decay products fly off at a 20 degree angle from the negative z axis (the choice of this angle is to ensure that the decay products pass through all three $3 \text{ m} \times 3 \text{ m}$ detection planes in the setup shown in Figure 2), and in the x-z plane (this is for simplicity). It was also assumed that

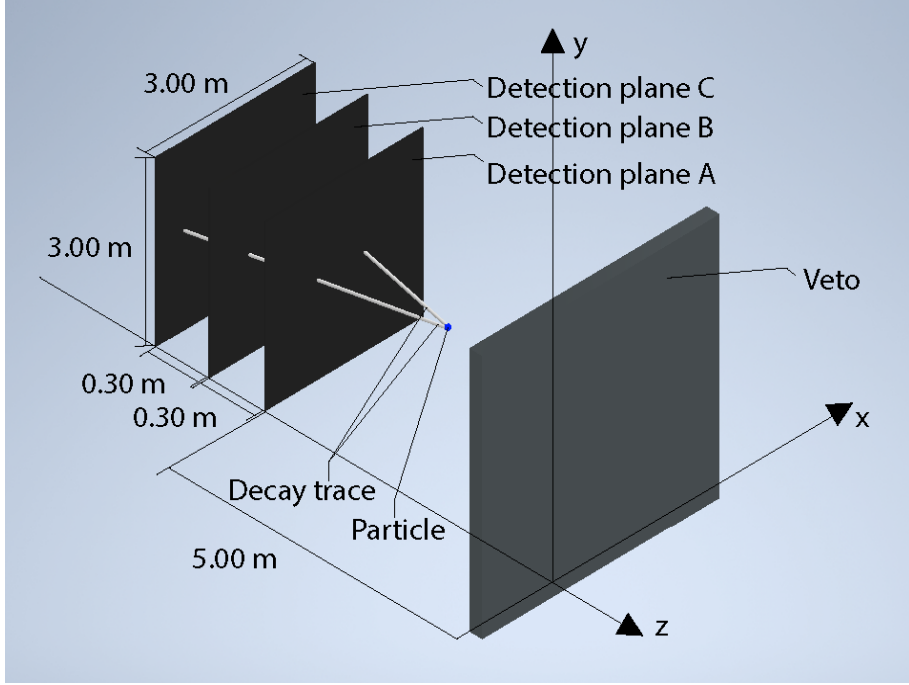


FIG. 2: Three-plane setup of the MAPP detector for a preliminary study of the reconstruction of the decay vertices of particles. The 'decay zone' is the area between the veto wall and the detection plane A.

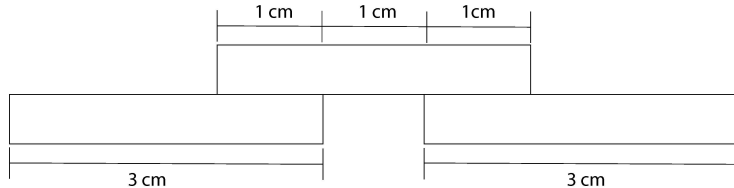


FIG. 3: overlapping of the scintillator planks as seen from one end.

the decay products follow a straight line. The coordinates of the intersection between the detection planes and the decay products lines/traces was found via a computer simulation. I call these points the 'reference points' (see Figure 5b), for reasons that will become obvious in Section IV. The trajectories of the two decay products are shown as two white traces in Figure 2. Points then are generated around the 'reference points' at the planes of detection by performing a Gaussian smearing with a computer program (see Figure 5c). At this stage, one can think of the 'reference points' as the points at the center of a square of the grid. This is not true though, but it gives a good idea of what one would observe in real life, as it is explained in Section V. The smearing was done for each axis (x and y). The parameters

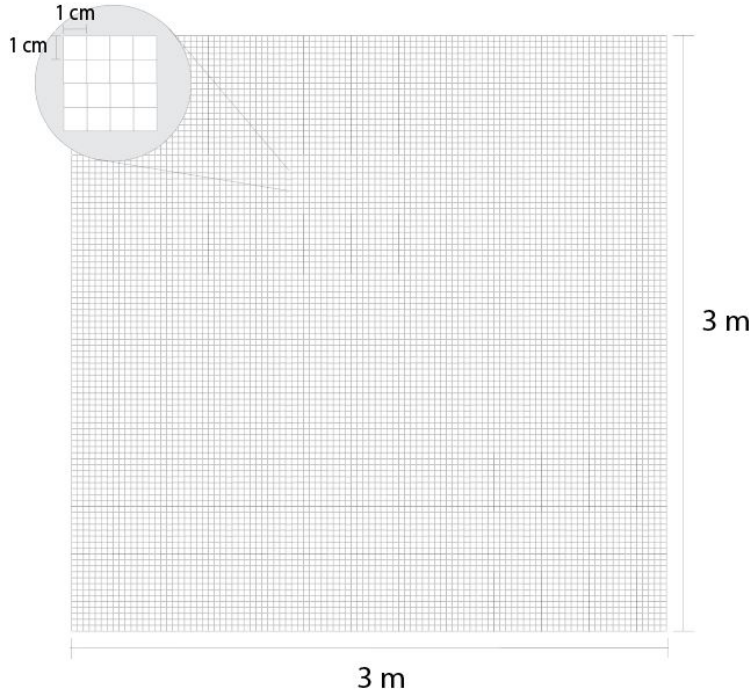


FIG. 4: Effective grid in each detection plane from the overlapping of scintillator strips.

used were the mean, which was taken to be the coordinate of the reference point (x or y), and the standard deviation, taken to be 0.005 m (0.5 cm). In this way, two ‘generated points’ are created (one per decay product) per detection plane. With these points at hand, the decay traces for the ‘generated points’ are built via a least-squares linear fit (see Figure 5d). From these traces, one can estimate the coordinates of the ‘generated vertex’. The distance between the ‘generated vertex’ and the ‘reference vertex’ gives the resolution of reconstruction of the decay vertex.

In the simulations, I have looked at 1000 decays, and I have calculated the distance between the vertices of the ‘reference decay’ and the ‘generated decay’. In the computer program, all the six ‘generated points’, and the subsequent traces and vertex reconstruction, were created and calculated, respectively, one decay at a time. So the distances between the ‘reference vertex’ and the ‘generated vertex’ are calculated one (generated) decay at a time. This was done through 1000 iterations of the computer program.

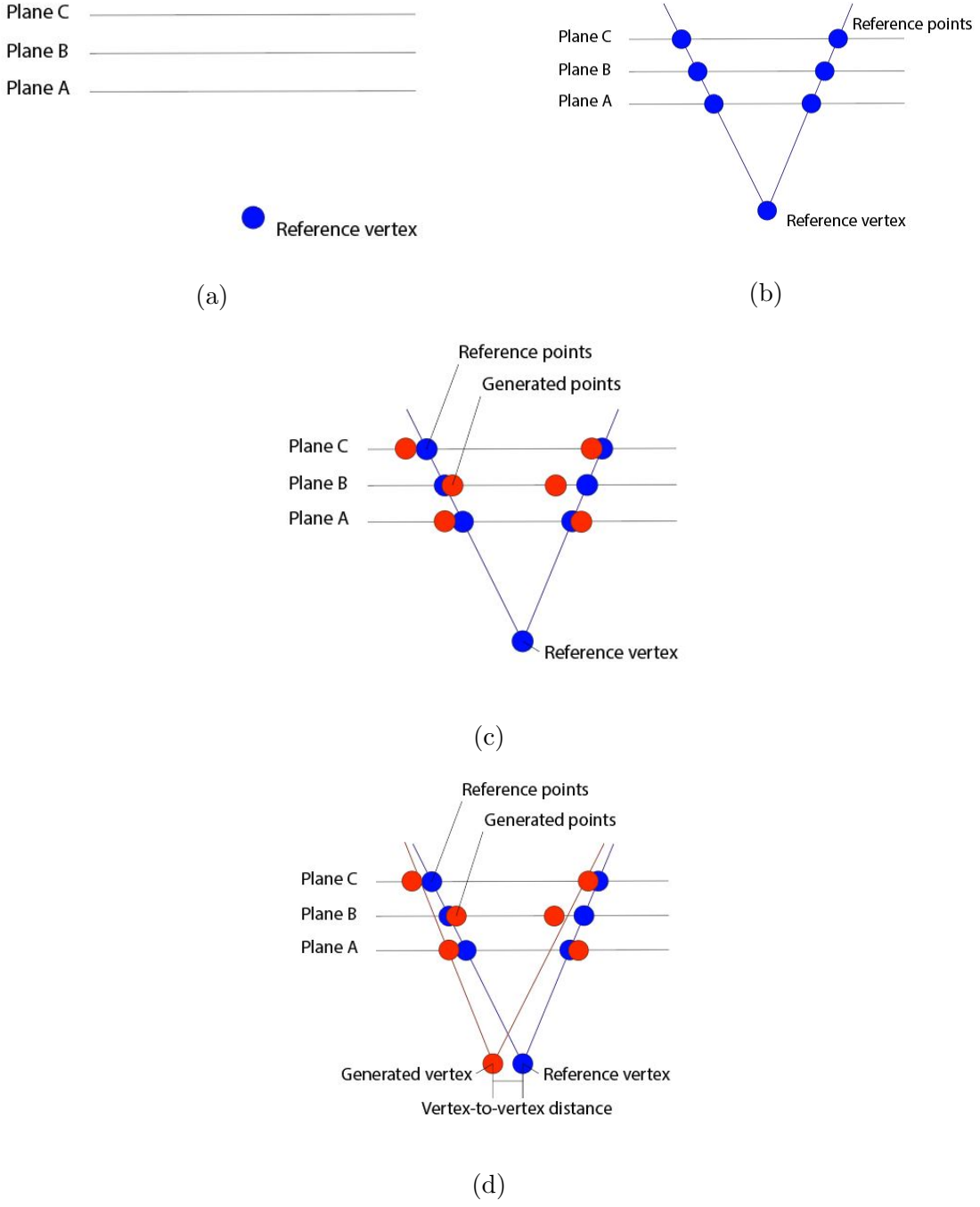


FIG. 5: (a) A ‘reference point’ is created in the middle of the ‘decay zone’. (b) Two decay traces are generated from this ‘reference point’, and the points of intersection of these traces with the detection planes (A, B and C) give the ‘reference points’. (c) A Gaussian smearing is performed around the reference points to create the ‘generated points’. (d) A ‘generated vertex’ is created by performing a least-squares fit of the ‘generated points’; the ‘generated vertex’ is (approximately) the point of intersection of the reconstructed decay traces from the Gaussian smearing.

B. Reduction of the noise in the apparatus

Part of this project also consisted in the study of the noise reduction in the apparatus to be used at the MAPP detector. The detection of particles is performed through the scintillator planks and photomultiplier tubes (PMs) attached to their ends. The light produced by the scintillator material upon being hit by an ionizing particle is registered by the PMs as a voltage signal, which one can readily observe with an oscilloscope. However, there is electronic noise inherent to the PMs. There are two type of PMs: photomultiplier tubes (PMTs) (see Figure 6) and silicon PMs (SiPMs) (see Figure 7); for this test, I used the latter (SiPMs), which are noisier and have smaller noise signals than the former. This part of the project looked at the size of the noise signals and how the overall noise is reduced by the number of SiPMs placed in coincidence. To explain further what one means by placing the PMs in coincidence, one can take a look at Figure 8.



FIG. 6: Photomultiplier tube.

In Figure 8: the SiPMs are placed under 28 volts (they can stand a maximum of 31 volts), and the amplifier power supply to its electronic board was set to 5 volts. At this point, the SiPMs are not attached to the scintillator material. They are under light-tight condition, so any signal produced by the SiPMs is from electronic noise. The size of the noise had a maximum value of approximately 9 mV. This signal was amplified (otherwise the discriminator could not read it) by 50; so, the signal sent to the discriminator was of a maximum of approximately 450 mV. The discriminator has a threshold that blocks signals that have a smaller size than the one set by the threshold regulator; this threshold was changed throughout the testing. In addition, the discriminator has a time window, or width, that blocks signals with a duration larger than the one set by the width regulator;

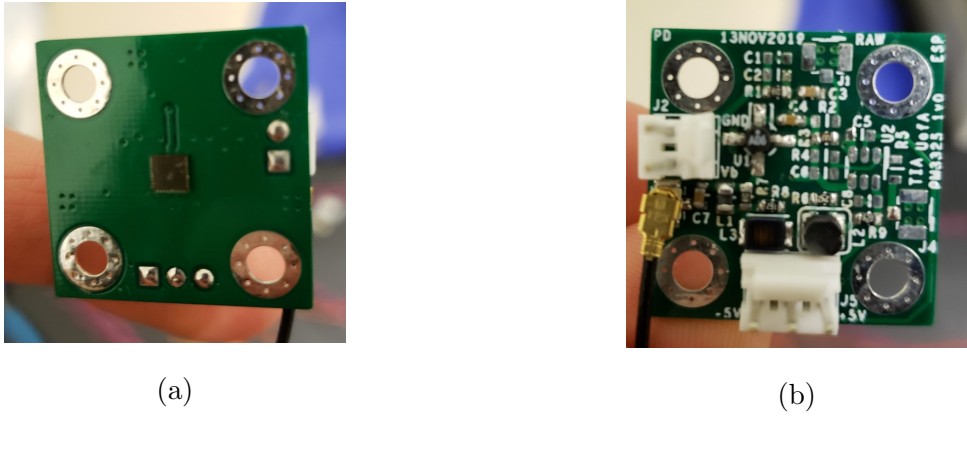


FIG. 7: Silicon photomultiplier (a) and its electronic board (built at the electronic shop at the University of Alberta) (b).

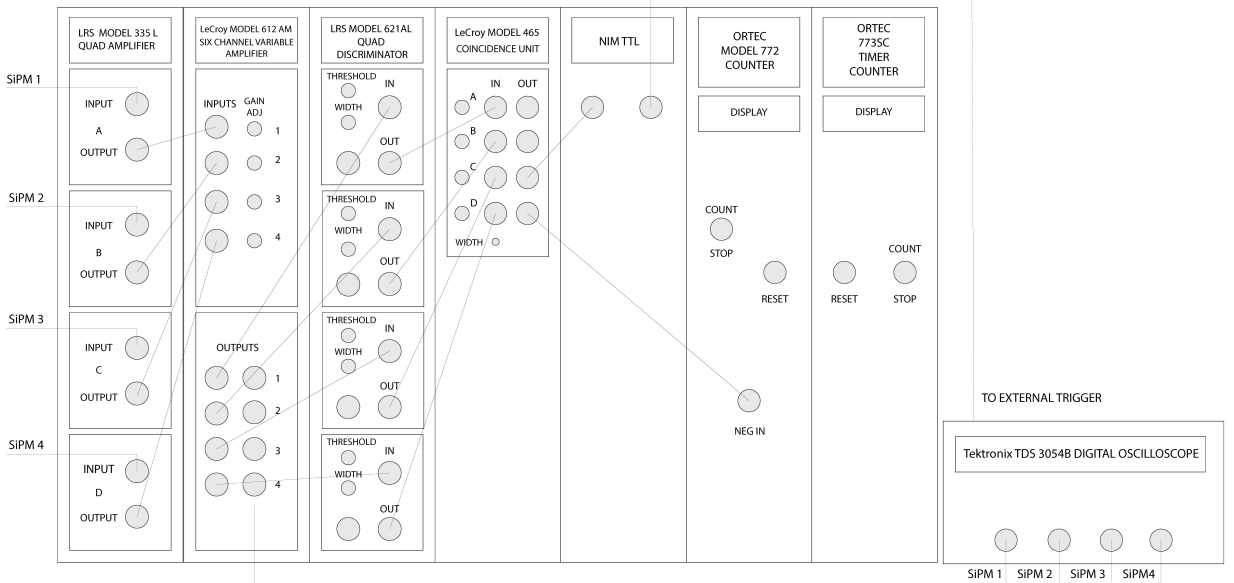


FIG. 8: Electronics setup for the noise reduction of SiPMs.

this width was set to 40 nanoseconds throughout the testing. Once the signals from the SiPMs have been filtered by the discriminator, they are sent to a coincidence unit. The coincidence unit has a time/coincidence window (width); for multiple signals that enter the coincidence unit inside the set time window (40 nanoseconds throughout the testing), the coincidence unit produces a signal. These signals are counted by a counter, and the counts are taken for a period of time (variable depending on the number of SiPMs placed in coincidence). For the visualization of the signals, the signal from the coincidence unit is

sent to an oscilloscope, which is triggered according to the times the coincidence unit sends a signal. At the same time, the signals from the different SiPMs are sent directly, after being amplified, to the oscilloscope; these appear in the oscilloscope's screen each time the coincidence unit is triggered.

The objective of this test was to determine the minimum threshold at the discriminator and the minimum number of SiPMs placed in coincidence at the which the number of counts from noise are cancelled. Having a free-noise equipment seems not to be possible, because of random events. However, this test will help maximize the efficiency of the scintillator plank to be used at MAPP (more on Section III).

C. Determination of the maximum possible dimensions of the detection walls at MAPP

The setup for this is shown in Figures ???. The scintillator strip is scanned by scintillator paddles. Photomultiplier tubes (PMTs) (refer to Figure 6) are attached to the paddles and SiPMs (refer to Figure 7), to one end of the scintillator strip. See Figure 10 for a picture of SiPMs attached to one end of the scintillator strip. The number of SiPMs installed on the scintillator strip is such that it minimizes the electronic noise (this was determined to be 4 SiPMs; also see Section III). The three PMs are put in coincidence, and the oscilloscope is triggered by the coincidence unit (refer to Figure 8). The signals of the SiPMs are sent directly to the oscilloscope. No amplification is needed for the PMTs, since their signals are more than 50 times larger than the signals produced by the SiPMs. The widths at the discriminator and coincidence units are set to 40 nanoseconds.

Every time the coincidence unit sends a signal to the oscilloscope (after being triggered by the four PMs detecting a cosmic-ray particle), one can see the size of the signals coming directly from the SiPMs. These signals coming directly from the SiPMs are expected to decrease in size as the paddles are moved away from the end where the SiPMs are attached to the scintillator strip. Eventually, the signal from the SiPMs will reach a value that is just above the determined threshold at which the noise is minimized (this was 2 mV; also see Section III); at that point, the location of the paddles along the scintillator strip will tell which is the maximum length of scintillator that one can use without losing any possible detection.

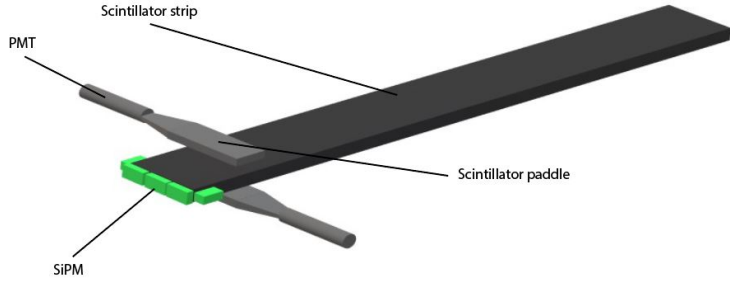


FIG. 9: Setup for the determination of the maximum possible length of the scintillator strip.

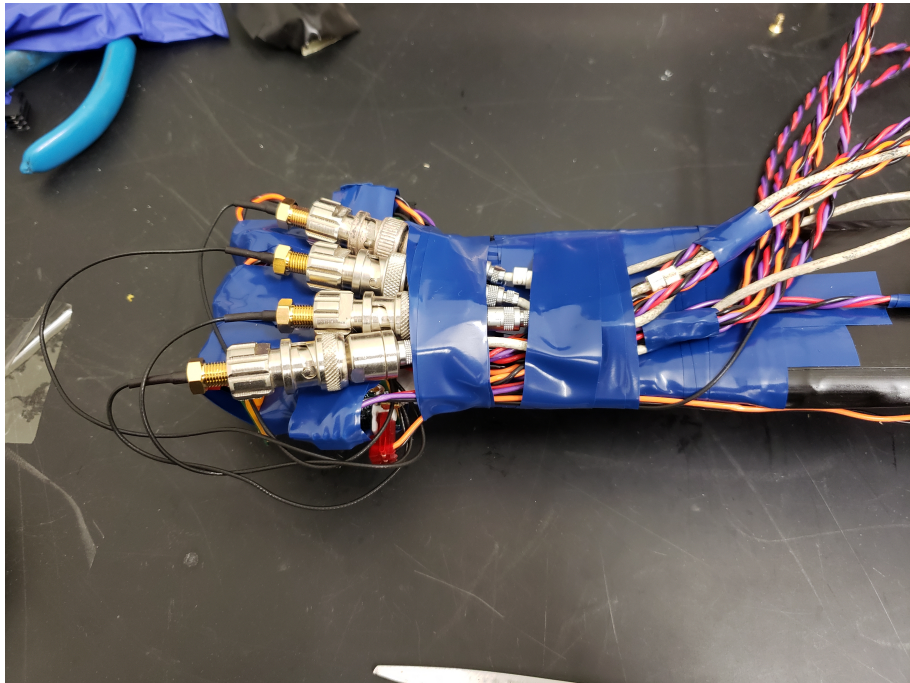


FIG. 10: Photograph of SiMPs (wrapped) attached to one end of the scintillator strip.

In order to discard random events, and to make sure that one is seeing a particle going through the two scintillator paddles and the scintillator strip, it was considered to place a source of ionizing radiation on top of one of the paddles. A candidate for this was Beryllium-8, for the emission of alpha particles.

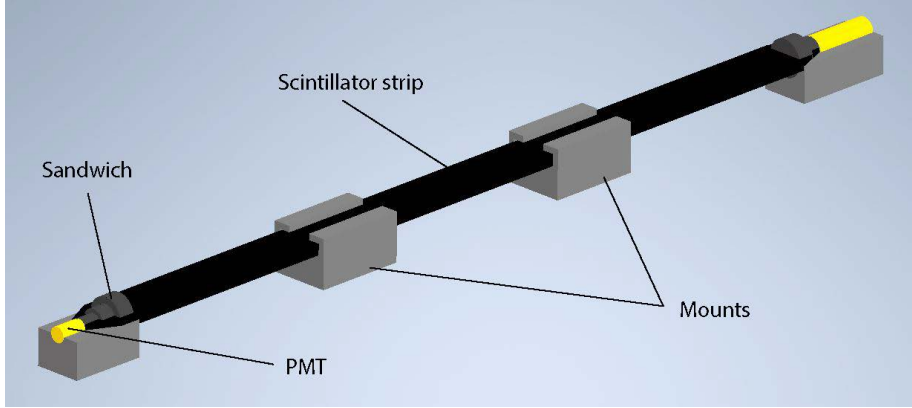


FIG. 11: Setup for the determination of the scintillator efficiency. The supports are placed to ensure that the scintillator strip is completely horizontal during the scanning with the scintillator paddles (which are shown in Figure 9). The sandwich creates a light-tight seal between the PMT and the scintillator strip's end.

D. Determination of the efficiency of the scintillator strip

The setup for this test is shown in Figure 11. PMTs are attached to each end of the scintillator strip, and the scintillator strip is scanned by scintillator paddles with PMTs attached to them. Figure 12 shows a photography of a preliminary test for the scanning of the scintillator strip with the scintillator paddles. The four PMTs are put in coincidence (refer to Fig 8). Their signals are not amplified, the width at the discriminator and coincidence units is kept to 40 nanoseconds, and the threshold at the discriminator unit is set to a maximum: 9 V (this is because the size of the noise signals from the PMTs is very large). The reason why PMTs are installed unto the scintillator strip instead of SiPMs in this setup, is that the noise signal size of the PMTs required attenuation when used with SiPMs, otherwise, the efficiency of the scintillator strip comes out very low. The setup shown in Figure 12 used SiPMs on the scintillator strip instead of PMTs. The idea is to make a noise reduction study for the four PMTs placed in coincidence as it was done for the SiPMs. One should be able to tell at which discriminator threshold the noise signals from the four PMTs put in coincidence are killed. For this one needs to find a way to attenuate the noise signals from the PMTs to bring them down to the voltage range that the discriminator's threshold can manage.

The formula for determining the efficiency of the scintillator strip is in Eq. 3. The number

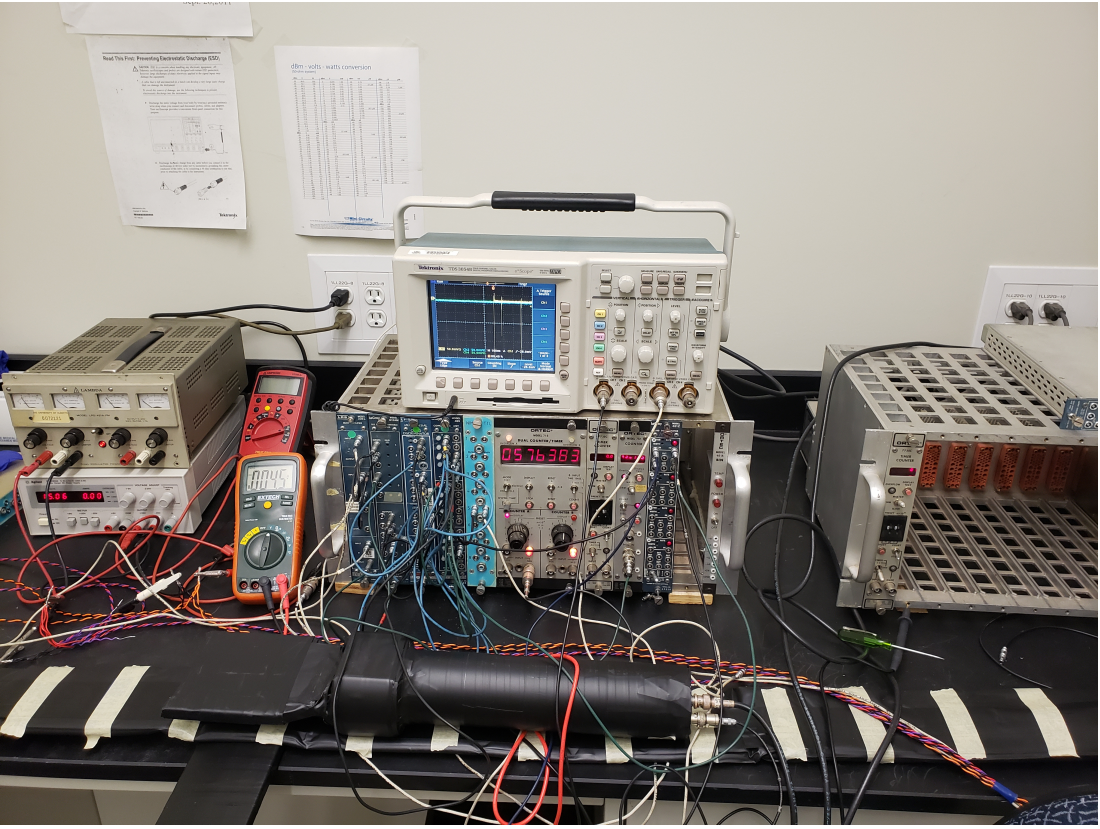


FIG. 12: Setup for the determination of the scintillator efficiency. This photography shows the setup in real life for a preliminary test of the efficiency of the scintillator strip. The mounts in Figure 11 had not been made. For this preliminary test, SiPMs were attached at the ends of the scintillator strip.

of times the PMTs are triggered approximately simultaneously is recorded by the counter unit over a period of time.

$$Efficiency = \frac{[2 \times PMTs(\text{strip}) + 2 \times PMTs(\text{paddles})] \# \text{ of coincidences}}{[2 \times PMTs(\text{paddles})] \# \text{ of coincidences}} \quad (3)$$

See Figure 13. The four PMTs are placed in coincidence, and the PMTs on the scintillator paddles are also placed in coincidence independently. One chooses a time frame, say 10 minutes, in which one registers the number of times the counter unit was triggered by the four PMTs triggering the coincidence unit and the two PMTs on the paddles triggering the coincidence unit as well. The counts from the 4-fold and 2-fold coincidences are done simultaneously. Because the size of the signals of the PMTs is larger (more than 50 times larger) than the signals from the SiPMs, the two scintillator paddles register a large number

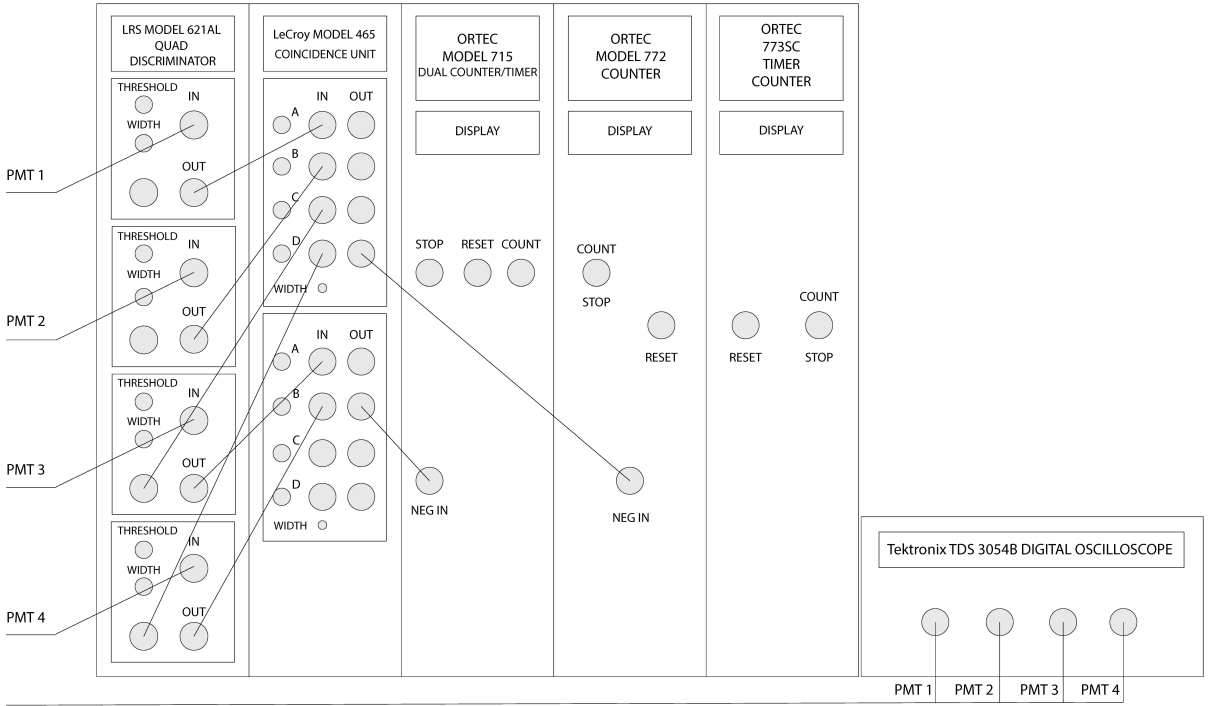


FIG. 13: Electronics setup for the determination of the scintillator’s efficiency.

of coincidence from noise, while the SiPMs would actually be recording real hits from cosmic rays (muons, specifically). The equipment would not allow for the attenuation of the signal coming from the PMTs, so the best solution to the problem exposed in the last lines was to use PMTs on the scintillator strip instead of SiPMs. In this way the noise from all the PMs is more or less matched.

E. Further exploration on the simulation of the detection of fractional charges

An LED is embedded into the scintillator material to simulate the detection of fractional charges.

IV. RESULTS AND ANALYSIS

A. The MAPP detector: exploration of the resolution in the reconstruction of decay vertices at the LHC

For the following, refer to Figure 2. A ‘reference (decay) vertex’ was created at the center of the ‘decay zone’ (i.e. the zone between the veto wall and the detection plane A). The coordinates for this point are: (1.50, 1.50, -2.50). It was assumed that the decaying particle was moving parallel to the negative z-axis. I was also assumed that the decaying particle decayed into two products, each one flying off in a straight line at a 20 degree angle from the negative z-axis, in the x-z plane. The intersection points between the traces of the decay products and detection planes were determined to be (these are the ‘reference points’; notice that all of them are inside the detection area, from $x = 0$ to $x = 3.00$ and $y = 0$ to $y = 3.00$):

Plane A:

Trace 1: (2.3899, 1.5000, -5.0000)

Trace 2: (0.5701, 1.5000, -5.0000)

Plane B:

Trace 1: (2.4991, 1.5000, -5.3000)

Trace 2: (0.4609, 1.5000, -5.3000)

Plane C:

Trace 1: (2.6083, 1.5000, -5.6000)

Trace 2: (0.3517, 1.5000, -5.6000)

- Gaussian smearing along the x axis (two-dimensional analysis)

Figure 14 shows the ‘reference decay’ and the ‘generated decay’ (from the Gaussian smearing along the x axis around the ‘reference points’). Figure 15 shows the histogram for the distances between the ‘reference vertices’ and the ‘generated vertices’.

Note that the distribution in Figure 15 is not a Poisson distribution. For a particular run of the program, the chi-square test rejected the null hypothesis at a 5% significance level.

The p-value was 6.6482e-28. Although the distribution is not Poissonian, in order to avoid picking up a value subjectively, I will use the Poisson parameter from this run to be the resolution in the reconstruction of the decay vertex in two dimensions: 0.062 ± 0.005 m.

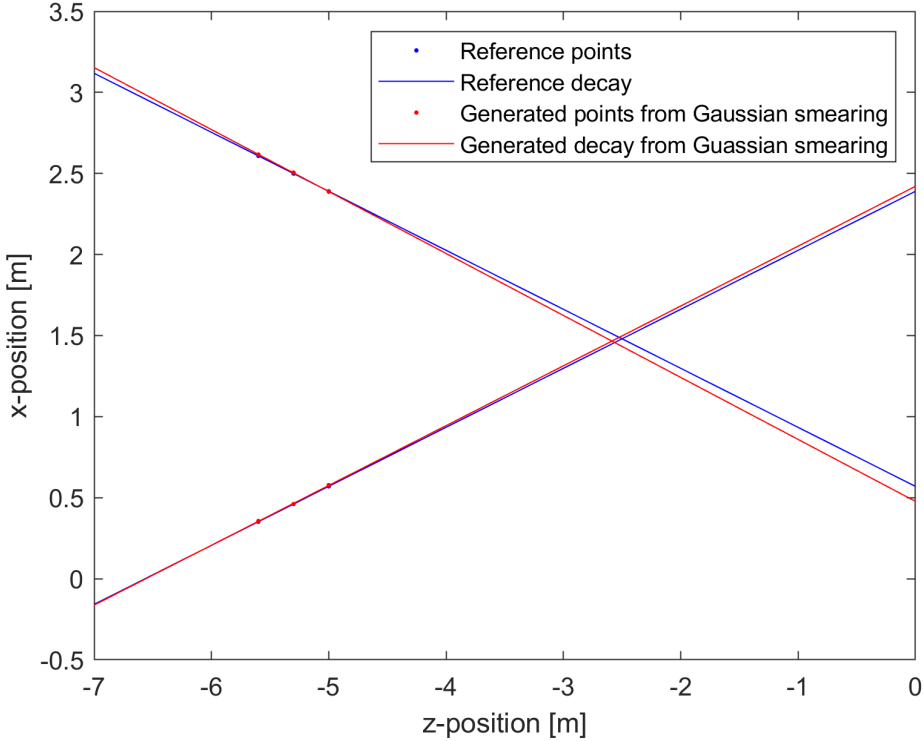


FIG. 14: From a particular iteration of the code: 'reference decays' and 'generated decays' for the study of the resolution of the vertex reconstruction for decays registered at the MAPP detector at the LHC in two dimensions.

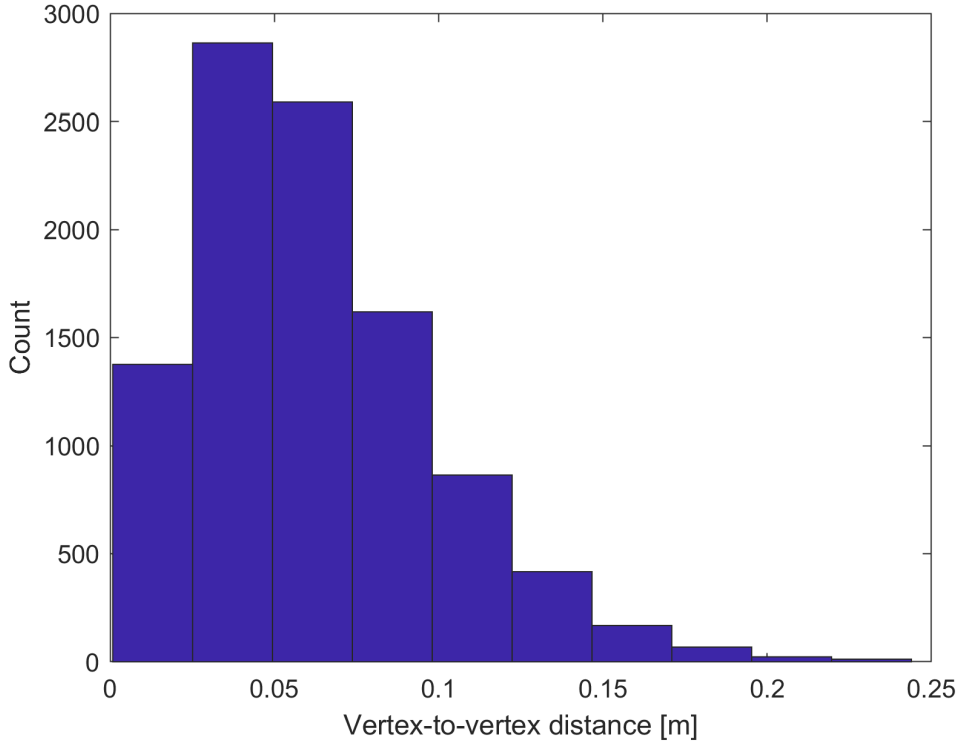


FIG. 15: Histogram of the distances between the ‘reference vertex’ and the 1000 vertices generated from a least-squares linear fit performed on the ‘generated points’ from a Gaussian smearing along the x axis around the ‘reference points’ with a standard deviation of 0.005 m.

- Gaussian smearing along both the x and y axes (three-dimensional analysis)

Figure 16 shows the ‘reference decay’ and the ‘generated decay’ (from the Gaussian smearing along both the x and y axes around the ‘reference points’). Figure 17 shows the histogram for the ‘reference vertices’ and the ‘generated vertices’. Important to mention is that the traces from the ‘generated decays’ do not always exactly intersect each other at a point (the expected ‘generated decay vertex’). In order to account for this, I calculated their point of intersection in the x-z plane, and then I assigned a y-coordinate point of intersection by determining the middle point in between the y-values of the two ‘generated decays’ at the point of intersection in the x-z plane.

As for the two-dimensional case, note that the distribution in Figure 17 is not a Poisson distribution. For a particular run of the program, the chi-square test rejected the null hypothesis at a 5% significance level. The p-value was 1.2412e-05. Although the distribution

is not Poissonian, in order to avoid picking up a value subjectively, I will use the Poisson parameter from this run to be the resolution in the reconstruction of the decay vertex in three dimensions: 0.069 ± 0.005 m.

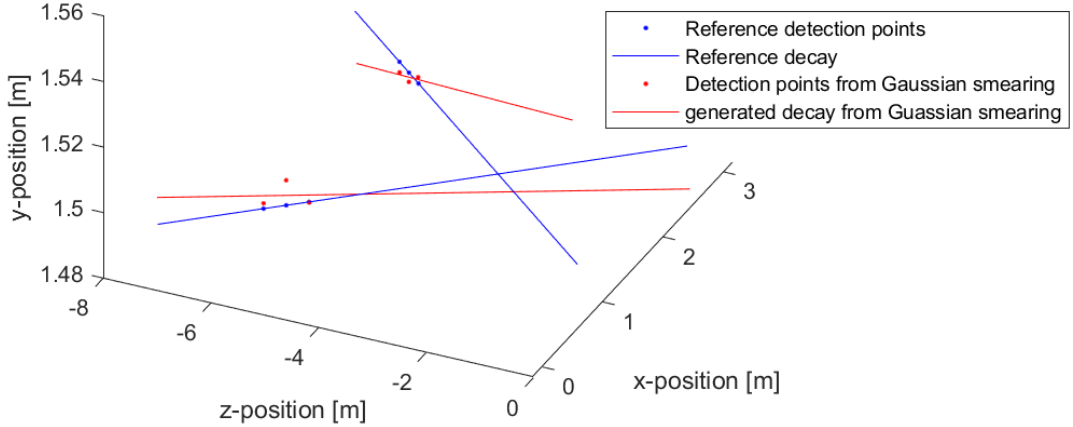


FIG. 16: From a particular iteration of the code: 'reference decays' and 'generated decays' for the study of the resolution of the vertex reconstruction for decays registered at the MAPP detector at the LHC in three dimensions.

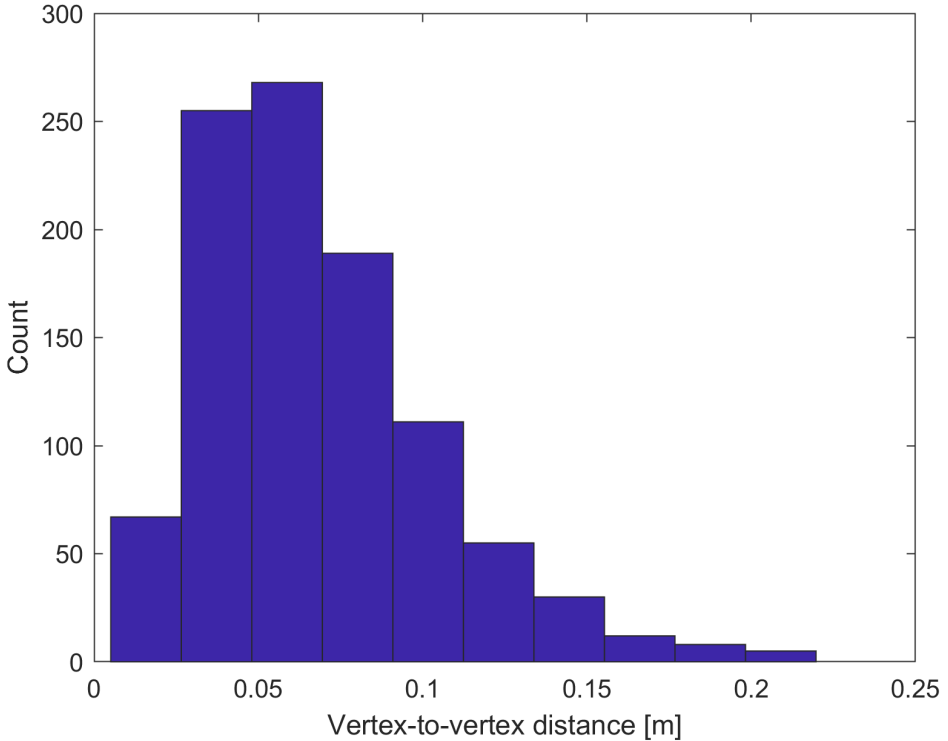


FIG. 17: Histogram of the distances between the ‘reference vertex’ and the 1000 vertices generated from a least-squares linear fit performed on the ‘generated points’ from a Gaussian smearing along the both the x and y axes around the ‘reference points’ with a standard deviation of 0.005 m.

B. Reduction of the noise in the apparatus

For the following, refer to Figure 8. To recall, the basic setup for the electronics was: SiPMs → amplifier (x50; biggest SiPM noise signal without amplification \approx 9 mV) → discriminator (time window \approx 40 ns; threshold was varied from 300 mV to 9V) → coincidence unit (time window \approx 40 ns) → counter. The results are summarized in Figure 18 (note that the amplification factor of 50 has been removed in the graph): the threshold at which the noise from the SiPMs is expected to be zero (the ‘killing threshold’) as the number of SiPMs put in coincidence increases tends to 1.1 mV (without amplification).

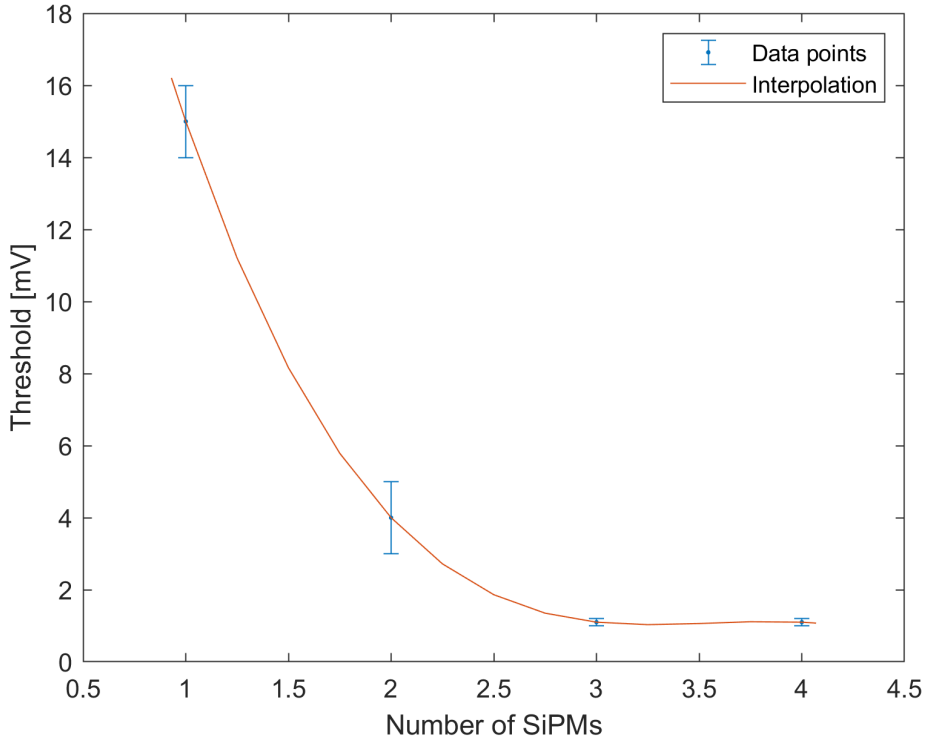


FIG. 18: Graph showing the threshold at which the noise from the SiPMs was killed per number of SiPMs put in coincidence.

V. DISCUSSION

A. The MAPP detector: exploration of the resolution in the reconstruction of decay vertices at the LHC

For the following, refer to Figure 2. It was previously assumed that the ‘reference points’ pass exactly through the center of the ‘detection squares’ they hit at the detection planes. This is not necessarily true. Nevertheless, the points that one would be able to ‘see’ at MAPP will be the ‘centered points’ (i.e. the points at the center of the ‘detection squares’). This is because of the way the detector is mounted (refer to Section III). The overlapping of the scintillator planks along the x and y axes can tell us which ‘detection square’ the decay product hit by looking at which PMs at the end of the scintillator planks through which the decay product passed were triggered (as explained in Section III). One would be able to tell only through which ‘detection square’ the decay product passed, but not the exact x and y coordinates of the intersection between the ‘detection plane’ and the decay product.

Simulation	Reality
‘Reference points’ exactly fit the ‘reference decay traces’	‘Real points’ (from the real decay) exactly fit ‘real decay traces’ (this is obvious)
‘Generated points’ used to create ‘generated decay traces’ (which they do not match exactly)	‘Centered points’ create decay traces (which are the same as the ‘reference decay traces’, and which they do no match exactly)

TABLE I: Equivalence of the simulation to what would happen in real life at MAPP.

Therefore, immediately, one assigns to the point of intersection between the ‘detection plane’ and the decay product the coordinates of the center of the ‘detection square’ that was hit.

Now assume that the ‘reference points’ exactly match the least-squares regression lines of some ‘centered points’ (see Figure 19). This is totally plausible, and therefore, the ‘reference vertex’ corresponds to the vertex that one would reconstruct at MAPP in real life. In Section IV it was calculated that the resolution capacity of the reconstruction of a decay vertex at MAPP, with the setup explained in Section III, would be of about 0.069 ± 0.005 m (in the more realistic three-dimensional analysis, where the Gaussian smearing was performed along both the x and y axes). This was done thinking of the ‘reference points’ as the points at the center of the ‘detection squares’ that were hit and the ‘generated points’ as the events one would see at MAPP. Of course, this is not true, but if now one thinks of the ‘centered points’ as the events that one would see at MAPP, then one can apply the results of Section IV to them, and say that the vertex reconstructed from the ‘centered points’ would be about 0.069 ± 0.005 m away from the real decay vertex.

There is no loss of generality here. It is enough to see the parallelism between the simulation and the real-life situation. This is summarized in Table I. Basically, one does the following ‘translations’: ‘reference points’ → ‘real points’, ‘generated points’ → ‘centered points’.

B. Reduction of the noise in the apparatus

It was established in Section IV that as the number of SiPMs put in coincidence increases, the ‘killing’ threshold tends to 1.1 mV (without amplification). Nevertheless, random fluc-

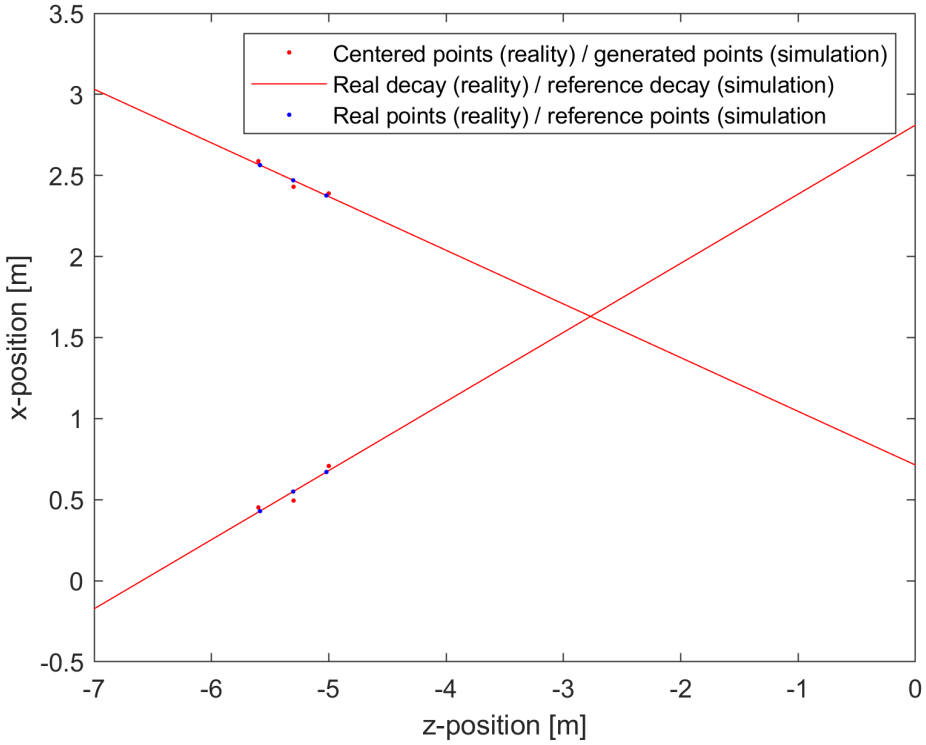


FIG. 19: ‘Reference points’ and ‘centered points’. The spacing between them was exaggerated for illustrative purposes. The ‘centered points’ correspond to the points at the center of the ‘detection square’ hit by the ‘reference points’.

tuations always occurred at this threshold, where one would expect zero noise according to Figure 18. Figure 18 also suggests that one would not reduce the ‘killing threshold’ by putting more than 4 to 5 SiPMs in coincidence. The test was done up to 4 SiPMs because of the limitations of the apparatus. I would suggest using a threshold of 2 mV (this for not amplified signals), and an amount of 4 or more SiPMs put in coincidence at the MAPP detector.

C. Determination of the maximum possible dimensions of the detection walls at MAPP

For this test it was necessary to build/acquire an interface between the oscilloscope and a computer, in order to record all the data for the times when the oscilloscope was triggered by the coincidence unit registering (approximately) simultaneous signals from the SiPMs on

the scintillator strip and the PMTs on the scintillator paddles arriving at the (coincidence) unit. The process of building/acquiring the interface for the acquisition of data was not finished due to time constraints caused by pressing external factors.

D. Determination of the efficiency of the scintillator strip

The ideal scenario was to use SiPMs attached to the ends of the scintillator strip. From the results in Section IV, four SiPMs would have been placed at each end of the scintillator strip, and the threshold (for the SiPMs only) at the discriminator unit would have been 2 mV (without amplification), as determined above (Section V). Nevertheless, the performance of the test with this setup would have required the building/acquisition of an attenuator of the signals coming from the PMTs. The signal size, just from noise, of the PMTs was larger than the maximum value that the discriminator unit's threshold could achieve (9 V).

The process of building/acquiring the attenuator was left unfinished because of pressing external factors. It was planned then to perform the measurement of the efficiency of the scintillator strip with PMTs attached its ends instead. In order to be able to do this, a sandwich had to be built in order to create a light-tight seal between the PMT and the scintillator strip (see Figure 11). The sandwich was necessary because the diameter of the cross section of the PMTs was larger than the thickness of the scintillator strip's cross section. The sandwich would block the light not coming from the scintillator. In addition, a mount for the sandwiches and a system that ensured that the PMTs and sandwiches would be tightly pressed against each other was needed to be created. The mounts for the sandwiches were designed completely. The mechanism for pressing the PMTs against the sandwiches was left unfinished because of pressing external factors. As mentioned in Section III, in addition to all this, a noise study similar to the one done with the SiPMs is necessary for the PMTs. By finding the minimal threshold at the discriminator for which the counter gives zero counts for the four PMTs placed in coincidence, one would make sure to be looking at signals from detected particles and not from noise.

VI. CONCLUSIONS

The prediction is that decay vertices at MAPP can be known to a resolution of 0.069 ± 0.005 m. This means that for a reconstructed decay vertex coordinate, the real position of the vertex is within a sphere of radius 0.069 ± 0.005 m around the reconstructed point. This is for the preliminary setup where three detection planes were used. This was for 3 cm wide scintillator strips being overlapped by 1 cm. A higher resolution is expected to be achieved by using thinner scintillator strips.

Tests on the determination of the maximum dimensions of the detection walls and the efficiency of the scintillator strip are currently being conducted. Preliminary results as of today (April 1st, 2020) indicate that the noise from the scintillator paddles put in coincidence is killed when their signals are passed through a threshold of 10.17 volts. Further work will be taken in the coming weeks.

-
- [1] Aad, G et al. (2012). Observation of a new particle in the search for the Standard Higgs boson with the ATLAS detector at the LHC. Physics Letters B, Volume 716, Issue 1, pp. 1-29, ISSN: 0370-2693. doi: <https://doi.org/10.1016/j.physletb.2012.08.020>.
- [2] Acharya, B; Alexandre, J.; Bendtz, K.;...; Pinfold, J. L. et al. (2016). Search for magnetic monopoles with the MoEDAL prototype trapping detector in 8 TeV proton-proton collisions at the LHC. Journal of High Energy Physics, Article number 67. doi: [https://doi.org/10.1007/JHEP08\(2016\)067](https://doi.org/10.1007/JHEP08(2016)067).
- [3] Blondel, A. (2002). The number of neutrinos and the Z line shape. Comptes Rendus Physique, Volume 3, Issue 9, pp. 1155-1164, ISSN 1631-0705. doi: [https://doi.org/10.1016/S1631-0705\(02\)01393-2](https://doi.org/10.1016/S1631-0705(02)01393-2).
- [4] Chatrchyan, S. et al (2012). Observation of a new boson at a mass of 125 GeV with the CMS experiment at the LHC. Physics Letters B, Volum 716, Issue 1, pp. 30-61, ISSN 0370-2693. doi: <https://doi.org/10.1016/j.physletb.2012.08.021>.
- [5] Davis, A. J. et al. (1989). Scintillating optical fiber trajectory detectors. Nuclear Instruments and Methods in Physics Research Section A: Accelerators, Spectrometers, Detectors and Associated Equipment, Volume 276, Issues 1-2, pp. 347-358, ISSN 0168-9002. doi: [https://doi.org/10.1016/0168-9002\(89\)90651-7](https://doi.org/10.1016/0168-9002(89)90651-7).
- [6] Frank, M.; de Montigny, M.; Ouimet, P-P. A.; Pinfold, J. L.; Shaa, A.; Staelsens, M. (2020). Searching for heavy neutrinos with the MoEDAL-MAPP detector at the LHC. Physics Letters B, v. 802, pp. 135204. ISSN 0370-2693. doi: <https://doi.org/10.1016/j.physletb.2020.135204>.
- [7] Giardino, P.P., Kannike, K., Masina, I. et al. (2014). The universal Higgs fit. Journal of High Energy Physics. 2014, Article number 46. doi: [https://doi.org/10.1007/JHEP05\(2014\)046](https://doi.org/10.1007/JHEP05(2014)046).
- [8] Griffiths, D (2008). Introduction to elementary particles. 2nd, revised ed. Weinheim: Wiley-VCH. Pp. 49, 51, 149-50.
- [9] Hasert, F.J.; ...; Pinfold, J.L et al. (1973). Search for elastic muon-neutrino electron scattering. Physics Letters B, Volume 46, Issue 1, pp. 121-124, ISSN 0370-2693. doi: [https://doi.org/10.1016/0370-2693\(73\)90494-2](https://doi.org/10.1016/0370-2693(73)90494-2).
- [10] Hasert, F. J. et al. (1973). Obervation of neutrino like interactions without muon or electron

- in the Gargamelle neutrino experiment. Physics Letters B, Volume 46, Issue 1, pp. 138-140, ISSN 0370-2693. doi: [http://10.1016/0370-2693\(73\)90499-1](http://10.1016/0370-2693(73)90499-1).
- [11] Ishiwata, K.; Wise, M. B. (2011). Higgs properties and fourth generation leptons. Physics Review D, Volume 84, Issue 5. American Physical Society. doi: <https://10.1103/PhysRevD.84.055025>.
- [12] McDonald, A. B. (2005). Evidence for neutrino oscillations I: solar and reactor neutrinos. Nuclear Physics A, Volume 751, pp. 53-66, ISSN 0375-9474. doi: <https://doi.org/10.1016/j.nuclphysa.2005.02.102>.
- [13] Moser, S. W et al. (1993). Principles and practice of plastic scintillator design. Radiation Physics and Chemistry, Volume 41, Issues 1-2, pp. 31-36, ISSN 0969-806X. doi: [https://doi.org/10.1016/0969-806X\(93\)90039-W](https://doi.org/10.1016/0969-806X(93)90039-W).
- [14] Pinfold, J.L. (2019). The MoEDAL Experiment at the LHC—A Progress Report. Universe 2019, 5, 47. doi: <https://doi.org/10.3390/universe5020047>.
- [15] Silenko, A. J. (2015). Spin precession of a particle with electric dipole moment: contributions from classical electrodynamics and from the Thomas effect. Physica Scripta, Volume 90m, Number 6, pp. 1-6. doi: <https://doi.org/10.1088/0031-8949/90/6/065303>.
- [16] Tanabashi, M. et al. (2018). Review of particle physics. Physical Review D, Volume 98, Issue 3. American Physical Society. doi: <https://doi.org/10.1103/PhysRevD.98.030001>.